Behaviour of FRP-to-Concrete Interfaces between Two Adjacent Cracks: A Numerical Investigation on the Effect of Bondline Damage

G.M. Chen[1]; J.F. Chen[2]; and J.G. Teng[3]

Abstract: The bond behaviour between FRP and concrete has been commonly studied using simple pull-off tests on bonded joints where an FRP plate bonded to a concrete prism is pulled at one end to induce debonding failure. Knowledge gained from such studies has been directly employed in predicting debonding failure in FRP-plated concrete beams induced by major flexural cracks, but significant differences exist between the two scenarios. The chief difference lies in the interaction between adjacent flexural cracks in a flexural member which is absent in a joint pull-off test. This interaction may be approximated using an FRP-to-concrete bonded joint where the FRP plate is pulled at both ends. This paper presents a numerical study into this bonded joint problem, with the main objective being to clarify the effect of bondline damage during slip reversals on the ultimate load. The study shows that such damage has a significant effect on the predicted bond behaviour and ultimate load when the ratio between the end loads is larger than 0.7, particularly when the bond length is reasonably large. An important implication of the present study is that in the modelling (e.g. finite element modelling) of debonding behaviour of FRP-plated RC beams where multiple cracks exist, the FRP-to-concrete interface should be represented using a bond-slip model with appropriate consideration of the damaged behaviour during slip reversals in order to achieve accurate predictions.

Keywords: Fiber reinforced polymers; Concrete beams; Bonding; Cracking; Damage; Finite element method.

---

1 Post-doctoral Research Fellow, Department of Civil and Structural Engineering, The Hong Kong Polytechnic University, Hong Kong, China

2 Reader in Structural Engineering, Institute for Infrastructure and Environment, School of Engineering, The University of Edinburgh, Edinburgh, United Kingdom

3 Chair Professor of Structural Engineering., Department of Civil and Structural Engineering, The Hong Kong Polytechnic University, Hong Kong, China (Corresponding author); Email: cejgteng@polyu.edu.hk

1. Introduction

External bonding of fibre-reinforced polymer (FRP) composites is a popular technique for strengthening concrete structures [1-4]. The performance of the bond between FRP and concrete is a key factor determining the behaviour of the strengthened structure [5-9]. Several failure modes in reinforced concrete (RC) members strengthened with FRP composites are directly caused by interfacial debonding between the FRP and the concrete. One of these failure modes, commonly referred to as intermediate crack debonding (IC debonding) [7, 9, 10], involves debonding of the FRP plate which initiates at a major flexural crack where the plate is under high tension and propagates along the FRP-to-concrete interface towards a stress-free end of the plate. The interfacial behaviour between FRP and concrete has been commonly studied using simple pull-off tests on bonded joints where an FRP plate bonded to a concrete prism is pulled at one end of the plate to induce debonding failure [10]. The pull-off tests can be categorized into different types as depicted in Fig. 1 [10, 11]. Many bond strength models have been developed for the FRP-to-concrete bonded joint based on different approaches. Among them, Chen and Teng's bond strength model which was developed based on a fracture mechanics solution and calibrated with a test database [10], was shown to be one of the most accurate models [12].

Teng *et al.* [13] developed an IC debonding strength model based on the bond strength model of Chen and Teng [10]. They assumed that IC debonding is driven by the critical flexural crack, and that the behaviour of the bond between the FRP plate and the concrete near the crack is similar to that in simple pull-off tests on FRP-to-concrete bonded joints. As a result, the IC debonding strength model of Teng *et al.* [13] has a form similar to that of the bond strength model of Chen and Teng [10], with a coefficient calibrated using a test database of IC debonding to reflect the differences between IC debonding in plated beams and debonding in simple pull-off tests.

Although Teng *et al.*'s IC debonding strength model was shown to have reasonably good accuracy [13], there are significant differences between debonding failure in a simple pull-off test and IC debonding failure in a plated RC beam. The chief difference lies in the interaction between adjacent cracks in a plated RC beam (Fig. 2) which does not exist in a simple pull-off test. Teng *et al.* [14] and Chen *et al.* [15] considered this interaction using a simple bonded joint model as shown in Fig. 3. This model is similar in geometry to a simple pull-off test but both ends of the FRP plate in the model (representing FRP at the positions of two adjacent cracks in a plated beam) are subjected to tension: P_1 at the right end and P_2 at the left end. Without loss of generality, it is assumed that $P_1 \geq P_2 \geq 0$. The concrete prism is assumed to be subjected to two forces, P_3 and P_4 at the right and the left ends (cracks) respectively. It is assumed that all these forces remain proportional throughout the loading process. The width, thickness and modulus of elasticity are denoted by b_p, t_p and E_p, respectively, for the plate, and by b_c, t_c and E_c, respectively, for the concrete prism. The length of the bonded part of the plate (i.e. bond length) is denoted by L. The adhesive layer is assumed to have a constant thickness and the whole model is assumed to be in a plane stress state. The deformation of the actual adhesive layer and those of a thin layer of the adjacent concrete is lumped together and referred to as the deformation of the interface (referred to as the "bondline" hereafter), which is assumed to be in pure shear because the failure mode of the interface is predominantly mode II interfacial fracture. It is further assumed that the two adherends, the plate and the concrete prism, are subjected to axial deformation only. Teng *et al.* [14] presented an analytical solution for this bonded joint based

on a bilinear local bond-slip model [Fig. 4(a)] between the FRP and the concrete. However, this solution is involved and does not provide an explicit expression for the ultimate load. Consequently, Chen *et al.* [15] developed a simpler analytical solution based on a linearly softening bond-slip model which neglects the ascending branch in the bilinear bond-slip model. They produced a simple yet fairly accurate solution in comparison with that given in Teng *et al.* [14].

In both of the above solutions [14, 15], the FRP-to-concrete bond-slip relationship was assumed to be fully reversible (referred to as undamaged model hereafter) [Fig. 4(a)]. This assumption is only accurate when the behaviour of the bondline is in the elastic regime. Since debonding failure in such FRP-to-concrete bonded joints commonly occurs in the concrete adjacent to the adhesive layer [11, 16], the descending branch of a bilinear bond-slip curve represents the behaviour of damaged concrete with micro-cracks. If local slip reductions (i.e. slip reversals) occur after the bondline has entered the softening stage (i.e. it has been damaged with micro-cracks), the bondline cannot be expected to regain its lost strength in all subsequent deformation. Reversed interfacial slips have been experimentally observed by Ueda et al. [16] and Sato et al. [17] and indentified as having a significant detrimental effect on bond behaviour, but there is still a lack of research on the mechanism of bond deterioration associated with slip reversals [18]. To clarify the effect of bondline damage on the predicted bonded joint behaviour using a numerical or analytical approach, a damaged bond-slip model with proper consideration of the effect of slip reversals needs to be used, but such a bond-slip model means that an analytical solution will become highly complicated. This paper presents a numerical study into the behaviour of the bonded joint between two cracks (Fig. 3) to clarify the effect of bondline damage associated with slip reversals on the bond behaviour of the joint.

2. Damaged Local Bond-slip Model

The bond-slip behaviour of FRP-to-concrete bonded joint is closely related to the behaviour of concrete under tension and shear [19]. For concrete under tension, it is common to assume either secant unloading or elastic unloading (see Fig. 5) with the former being more popular. The real cyclic behaviour of cracked concrete is much more complex and the actual unloading curve may lie between these two extreme cases [20-25].

A number of studies have been conducted on the unloading and cyclic bond-slip behaviour of FRP-to-concrete bonded joints [26-29]. It has been observed in these studies that: 1) when the interface has entered the softening range, the bond stress reduces as the interfacial slip decreases due to unloading; 2) the unloading stiffness decreases rapidly with the increase of interfacial slip at unloading; and 3) in the softening range, the unloading stiffness is generally smaller than the initial loading stiffness.

In the early stage of this study, a preliminary numerical investigation using a meso-scale finite element model similar to that in Chen et al. [30] was carried out; and the numerical results showed that the unloading behaviour of the FRP-to-concrete bonded joint is not only related to the unloading stiffness of the cracked concrete under tension, but also affected by the recovery of stiffness upon the closure of concrete cracks. The unloading curve of the bond-slip behaviour may lie between the two extremes of secant unloading and elastic unloading similar to the tensile behaviour of concrete as shown in Fig. 5. The actual bond-slip relationship under cyclic loading can be very complex, with nonlinear unloading and reloading behaviour; such a bond-slip model is yet to be developed [18]. As a result, a bi-linear bond-slip model with secant unloading (i.e. linear damage model and referred to

hereafter as the damaged model) as shown in Fig. 4(b) was adopted in this study. This model is simple for implementation but captures the key unloading features experimentally observed as mentioned above, providing sufficient accuracy for the purpose of the present study. Similar models have also been adopted in several studies on the modelling of FRP-concrete interfaces [18, 31-35].

3. Finite Element Modelling

3.1. The Finite Element Model

A finite element (FE) computational model as shown in Fig. 6(a) was proposed to simulate the FRP-to-concrete bonded joint model with the FRP plate being pulled at both ends (Fig. 3). The FE model was implemented in the FE software package ABAQUS [36]. In the model, the FRP plate and the concrete prism were idealised as truss elements (T2D2 [36]) with their bending effects neglected, based on the assumption that the two adherends of the FRP-to-concrete bonded interface (i.e. the plate and the concrete prism) are subjected to axial deformation only as described in Section 1. The truss element has the axial stiffness of either the FRP plate or the concrete prism as appropriate. As the bondline between the FRP and the concrete prism is assumed to be under pure shear deformation which represents the lumped deformation of the actual adhesive layer and that of a thin layer of the adjacent concrete as described earlier, it was modelled using the 4-node, two-dimensional interfacial cohesive element COH2D4 [36]. The cohesive elements share common nodes with the truss elements representing the FRP and with those representing the concrete prism. The constitutive properties of the cohesive elements include [36]: (a) the initial elastic stiffness; (b) the damage initiation point; and (c) the damage elevation law. For the bi-linear bond-slip model with linear damage as shown in Fig. 4(b), these properties can be determined as follows.

The initial stiffness:

$$K_0 = \frac{\tau_f}{\delta_1} \tag{1}$$

The damage initiation point is determined by the slip value δ_1 at which the peak shear stress (τ_m) is reached. The damage elevation law is described by a scalar damage variable, D, which is defined by the following expression proposed by Camanho and Davila [37]:

$$D = \frac{\delta_f(\delta_m - \delta_1)}{\delta_m(\delta_f - \delta_1)} \tag{2}$$

where δ_m is the value of slip at the initiation of unloading.

With the above expressions, the stress at the slip value of δ_m can be expressed as:

$$\sigma_m = (1 - D)K_0\delta_m \tag{3}$$

and the unloading stiffness K_m at the slip value of δ_m is

$$K_m = (1 - D)K_0 \tag{4}$$

It should be noted that the properties of the cohesive elements are independent of its nominal thickness if "traction-separation" type constitutive law is used [36]. A nominal thickness of 1 mm was adopted in this study (Fig. 6). All the results presented in this paper were obtained using the arc-length method which is capable of obtaining the full-range load-displacement response of the bonded joint as shown later.

3.2. Reference Case

In the numerical examples presented later in the paper, the following reference parameters were used unless otherwise stated: (a) geometrical and material parameters being those of a series of simple pull-off tests of FRP-to-concrete bonded joints by Yao *et al.*[11]: nominal thickness of FRP sheet $t_p = 0.165$ mm, width of FRP sheet $b_p = 25$ mm, thickness of the concrete prism $t_c = 150$ mm, width of the concrete prism $b_c = 150$ mm, elastic modulus of the FRP sheet $E_p = 256$ GPa, elastic modulus of concrete $E_c = 28.6$ GPa and concrete cylinder compressive strength $f_c' = 22.9$ MPa ; (b) local bond-slip parameters as deduced from the experimental load-displacement curve of a typical specimen (namely specimen II-5, see Yuan et al. 2004): $\delta_f = 0.16$ mm, $\delta_1 = 0.034$ mm, $\tau_f = 7.2$ MPa and $G_f = 0.58$ N/mm; (c) load ratios: $\beta = P_2/P_1 = 0.8$ and $\mu = P_3/P_1 = 1$; and (d) bond length $L = 100$ mm, which represents a typical crack spacing in RC beams [14]. For the reference case, numerical results not presented in this paper indicated that the effect of the axial stiffness of the concrete prism on the predicted joint behaviour is negligible. As a result, a simplified FE model as shown in Fig. 6(b) was used to produce the numerical results given next.

3.3. Mesh Convergence and Model Verification

Fig. 7 shows the numerical results for a bonded joint with $L = 100$ mm and a load ratio $\beta = 0$ (i.e. with $P_2 = 0$) which represents a simple pull-off test. In this case, the debonding process starts at the right end (i.e. the loaded end) and propagates towards the left end without involving any local slip reversal. As a result, the use of either of the two bond-slip models shown in Fig. 4 leads to the same prediction. Results from two different meshes with element lengths $m = 1$ mm and 0.5 mm respectively, as well as results from the analytical solution of Yuan *et al.* [38] are compared in Fig. 7. The results from all three sources are almost identical; the predicted maximum values of P_1 differ by less than 0.1%. Numerical results not presented here showed that a similar conclusion on mesh sensitivity can be reached for cases with $\beta > 0$ (e.g. $\beta = 0.8$). A mesh with $m = 1$ mm was thus used to obtain the results presented in the remainder of the paper.

4. Numerical Results

4.1. Effect of Bond Length

Fig. 8(a) shows the effect of the bond length L on the ultimate value of $P_{1,u}$. It has been observed by Teng et al. [14] that $P_{1,u}$ firstly increases with L but remains constant after L reaches a certain value. When the load ratio β is very small, this relationship remains valid despite the use of the damaged bond-slip model. However, for large β values (e.g. $\beta > 0.7$), $P_{1,u}$ firstly increases with L and reaches a peak value before it decreases to a constant value as L further increases. This phenomenon is more pronounced when β is close to 1. This may be explained as follows.

Since it is assumed that $P_1 > P_2$, $\beta = P_2/P_1$ has values varying between 0 and 1. When β is large and the bond length is long (so that P_1 does not interact with P_2 initially), a large P_2 leads to the softening of part of the bondline near the left end under the action of P_2. As the softening front (corresponding to the peak interfacial bond stress) from the right end propagates towards the left end, the bondline near the left end experiences local slip reversals.

This means that part of the bondline near the left end has been damaged before it is called upon to resist the differential between P_1 and P_2 and due to the prior damage, it cannot resist as much of this differential as a non-damaged bondline. For a given large β value, an increase of the bond length L leads to a larger reduction of the load-carrying capacity (compared to that predicted using the undamaged bond-slip model) because the bondline near the left end is now more severely damaged [Fig. 8(a)].

By contrast, when β is small (so is P_2), the bondline near the left end is still elastic and has not been damaged when the softening front from the right end arrives. Therefore, the resistance offered by the bondline near the left end to the differential between P_1 and P_2 has not been affected by prior damage and further analyses not presented here showed that the numerical results obtained from FE analysis are nearly identical to the analytical solution of Teng *et al.*[14]; in this case (i.e. small β) the analytical solution presented in Teng *et al.* [14] provides very accurate predictions.

The same results are alternatively presented in Fig. 8(b), where the bond length L is normalized against the characteristic softening length a_u which is defined in Teng *et al.* [14] as:

$$a_u = \frac{1}{\lambda_2}\arccos(\beta) \tag{5}$$

where

$$\lambda_2 = \sqrt{\frac{\tau_f}{\delta_f - \delta_1}\left(\frac{1}{E_p t_p} + \frac{b_p}{b_c E_c t_c}\right)} \tag{6}$$

in which t_p and t_c are the thicknesses of the FRP plate and the concrete prism respectively, b_f and b_c are the widths of the FRP plate and concrete prism respectively (see Fig. 3), E_p and E_c are the elastic moduli of the FRP plate and concrete respectively, f_c' is the concrete cylinder compressive strength, τ_f is the maximum bond stress of the bond-slip relationship, δ_1 is the interfacial slip corresponding to τ_f, and δ_f is the interfacial slip where the interfacial bond stress decreases to zero (see Fig. 4).

It is seen that all curves with $\beta > 0.5$ reach their peak values at about $L/a_u = 1.2$. For smaller β values, the peak is reached at slightly larger L/a_u values (with $L/a_u \approx 1.6$ for $\beta = 0.0$). For β values less than about 0.7, the numerical results are in agreement with the conclusion drawn from the analytical solutions of Teng *et al.* (2006) and Chen et al. (2007a) that an effective bond length (see Chen and Teng 2001) exists and a bond length longer than the effective bond length cannot increase (but also does not reduce) the ultimate load. For higher values of β, the present results indicate that an optimum bond length instead an effective bond length exists, and a longer bond length is detrimental to the ultimate load of the interface. This is an important phenomenon that arises from the effect of bondline damage.

4.2. Effect of Load Ratio β

Fig. 9 shows that the ultimate load $P_{1,u}$ increases with β when L is constant. This trend is more pronounced when $\beta > 0.7$. It is of interest to note that when β is sufficiently large

($\beta > 0.95$), $P_{1,u}$ is higher for a smaller L value. This is because at the same β value a smaller L means a smaller softening zone near the left end and less damage to the bondline there (the effect of damage is discussed in more detail later). This phenomenon is different from the prediction of the analytical solution of Teng *et al.* (2006) where the bond length has almost no effect when $\beta > 0.95$.

4.3. Effect of Damage

In Figs 10(a) and 10(b), the full-range load-displacement responses from the undamaged model and the damaged model for $\beta = 0.5$ and $\beta = 0.8$ respectively are compared. For each β value, numerical results of three different bond lengths (i.e. $L = 15$, 50 and 100 mm) are shown. It should be noted that the curves of the undamaged model were obtained based on Teng et al.'s (2006) analytical solution, while those of the damaged model were obtained from the proposed FE Model as shown in Fig. 6. For $\beta = 0.5$, the two curves of the undamaged model and the damaged model coincide with each other for the full range of the curves, independent of the bond length. For $\beta = 0.8$, the two curves fully coincide with each other only for a very small bond length $L = 15$; for larger bond lengths ($L = 50$ and 100 mm), the two curves coincide with each other before P_1 reaches the plateau: they diverge increasingly thereafter as the damaged bondline near the left end starts to have a significant effect, and the undamaged model leads to a higher $P_{1,u}$ than the damaged model. The above phenomena can be explained as follows.

Fig. 11 shows the interfacial shear stress distribution at different load levels for three different cases. Fig. 11(a) shows the case of L = 10 mm and β = 0.5: for all the load levels shown, the shear stress distribution of the undamaged model and the damaged model coincides with each other. More detailed analyses showed that this is because the bondline near the left side with a lower load (i.e. P_2) does not enter the softening range before the local slip reversal caused by the interaction of the two loads; the two curves at the load level of 5 kN illustrate this situation. As a result, the damage has no effect on the interfacial behaviour and the full range load-displacement responses from the damaged model and the undamaged model are nearly the same. Fig. 11(b) shows the case of $L = 15$ mm and $\beta = 0.8$. Similar observations as those of $L = 100$ mm and $\beta = 0.5$ can be made.

Fig. 11(c) shows the case of $L = 100$ mm and $\beta = 0.8$. Before P_1 reaches the plateau [cf. Fig. 10(b)], the two bond-slip models do not produce any difference in the shear stress distribution as shown by the two curves at $P_1 = 5$ kN. The shear stress peaks on the right and on the left are far apart and no local slip reversal has occurred at this stage. Note that the shear stress peaks also represent the fronts of the softening zones on the right and the left respectively and they are referred to as the softening fronts in this paper. When P_1 increases to 7 kN, the right softening front moves into the left zone where the bondline has already been damaged (or softened) under P_2. The damaged and undamaged bond-slip models lead to different interfacial stress distributions in this case because part of the left softening zone has experienced slip reversals. The damaged model also leads to a slightly smaller debonded zone on the right (where the interfacial shear stress is zero) because the bondline on the left is weaker (damaged) in this case so a longer bond length is mobilized to resist the load difference between P_2 and P_1 [Fig. 11(c)]; the weaker bondline on the left for the damaged bond model also leads to an earlier interaction between P_2 and P_1 (i.e. part of P_1 is

counterbalanced directly by part of P_2 through the FRP). This explains why the damaged model leads to a smaller displacement at the right end at the same load level above the plateau [Fig. 10(b)]. A similar phenomenon is also shown when the load reaches the ultimate load $P_{1,u}$ (≈ 9 kN for the undamaged model and ≈ 8.6 kN for the damaged model).

4.4. Comparison with Chen et al.'s Analytical Solution

The ultimate load in Figs 8(b) and 9 can be normalised against Chen *et al.*'s analytical solution [15] to compare the two solutions. Note that Chen *et al.* [15] presented an explicit expression for the ultimate load of the FRP-to-concrete interface with nearly the same accuracy as the solution of Teng *et al.*[14]. The normalized results are shown in Figs 12(a) and 12(b). Fig. 12(a) shows that the effect of damage is significant when $L/a_u > 1.2$ and $\beta > 0.7$. Note that the damage has no effect when $\beta = 0$ as no slip reversal is involved. However, since a linearly softening bond-slip model was used in Chen *et al.* [15] instead of a bi-linear model, despite the use of the same interfacial fracture energy in the FE model and Chen *et al.*'s model, they do result in minor differences when the bond length is very small [15]. This explains why the values are not exactly equal to 1 for $\beta = 0$ in Fig. 12(a). Fig. 12(b) shows more clearly that the damage to the bondline has a significant effect on the ultimate load when $\beta>0.7$.

5. Conclusions

This paper has presented a numerical investigation into the debonding behaviour of an FRP-to-concrete bonded joint when the FRP plate is loaded in tension at both ends, with the main objective being to clarify the effect of the damage of the bondline during slip reversals on the ultimate load of the bonded joint. The study has shown that such damage has a significant effect on the predicted bond behaviour and ultimate load when the ratio between the loads at the two ends of the FRP plate is larger than 0.7, which is especially true when the bond length is large. Apart from enhancing our understanding of the mechanics of failure of bonded joints, an important consequence of the conclusion from the present study is that in the modelling (e.g. finite element modelling) of debonding behaviour of FRP-plated RC beams where multiple cracks exist, the FRP-to-concrete interface should be represented using a bond-slip model with appropriate consideration of the damaged behaviour during slip reversals in order to achieve accurate predictions.

Acknowledgements

The authors are grateful for the financial support received from the Research Grants Council of the Hong Kong SAR (Project No: PolyU 5151/03E) and The Hong Kong Polytechnic University provided (Project code: BBZH). They would also like to acknowledge the support from the Scottish Funding Council for the Joint Research Institute between the University of Edinburgh and Heriot-Watt University which forms part of the Edinburgh Research Partnership in Engineering and Mathematics (ERPem).

References

[1] Bank LC. Composites for Construction: Structural Design with FRP Materials. Chichester, West Sussex, UK: John Wiley and Sons; 2006.

[2] Hollaway LC, Teng JG. Strengthening and Rehabilitation of Civil infrastructures Using Fibre-reinforced Polymer(FRP) Composites. Cambridge England: Woodhead Publishing Limited; 2008. p. 398.

[3] Oehlers DJ, Seracino R. Design of FRP and Steel Plated RC structures: Retrofitting

Beams and Slabs for Strength, Stiffness and Ductility. UK: Elsevier; 2004.
[4] Teng JG, Chen JF, Smith ST, Lam L. FRP-Strengthened RC Structures. Chichester, West Sussex, UK: John Wiley and Sons; 2002.
[5] Aprile A, Spacone E, Limkatanyu S. Role of bond in RC beams strengthened with steel and FRP plates. J Struct Eng-ASCE. 2001;127(12):1445-52.
[6] Buyukozturk O, Gunes O, Karaca E. Progress on understanding debonding problems in reinforced concrete and steel members strengthened using FRP composites. Constr Build Mater. 2004;18(1):9-19.
[7] Lu XZ, Teng JG, Ye LP, Jiang JJ. Intermediate crack debonding in FRP-strengthened RC beams: FE analysis and strength model. J Compos Constr. 2007;11(2):161-74.
[8] Rosenboom O, Rizkalla S. Modeling of IC debonding of FRP-strengthened concrete flexural members. J Compos Constr. 2008;12(2):168-79.
[9] Teng JG, Chen JF. Mechanics of debonding in FRP-plated RC beams. Proc Inst Civil Eng-Struct Build. 2009;162(5):335-45.
[10] Chen JF, Teng JG. Anchorage strength models for FRP and steel plates bonded to concrete. J Struct Eng-ASCE. 2001;127(7):784-91.
[11] Yao J, Teng JG, Chen JF. Experimental study on FRP-to-concrete bonded joints. Compos Pt B-Eng. 2005;36(2):99-113.
[12] Lu XZ, Teng JG, Ye LP, Jiang JJ. Bond-slip models for FRP sheets/plates bonded to concrete. Eng Struct. 2005;27(6):920-37.
[13] Teng JG, Smith ST, Yao J, Chen JF. Intermediate crack-induced debonding in RC beams and slabs. Constr Build Mater. 2003;17(6-7):447-62.
[14] Teng JG, Yuan H, Chen JF. FRP-to-concrete interfaces between two adjacent cracks: Theoretical model for debonding failure. Int J Solids Struct. 2006;43(18-19):5750-78.
[15] Chen JF, Yuan H, Teng JG. Debonding failure along a softening FRP-to-concrete interface between two adjacent cracks in concrete members. Eng Struct. 2007;29(2):259-70.
[16] Ueda T, Yamaguchi R, Shoji K, Sato Y. Study on behavior in tension of reinforced concrete members strengthened by carbon fiber sheet. J Compos Constr. 2002;6(3):168-74.
[17] Sato Y, Ueda T, Shoji K. Tension stiffening effect of reinforced concrete member strengthened by carbon fiber sheet. Bond in Concrete - from research to standards - Proceedings Budapest University of Technology and Economics, Budapest, Hungary2002. p. 606-13.
[18] Farah K, Sato Y. Uniaxial Tension Behavior of Reinforced Concrete Members Strengthened with Carbon Fiber Sheets. J Compos Constr. 2011;15(2):215-28.
[19] Lu XZ, Ye LP, Teng JG, Jiang JJ. Meso-scale finite element model for FRP sheets/plates bonded to concrete. Eng Struct. 2005;27(4):564-75.
[20] Feenstra PH. Computational Aspects of Biaxial Stress in Plain and Reinforced Concrete: PhD thesis, Delft University of Technology; 1993.
[21] Rots JG. Computational Modeling of Concrete Fracture: PhD Thesis, Delft University of Technology; 1988.
[22] Rots JG, Blaanwendraad J. Crack models for concrete: discrete or smeared? Fixed, multi-directional or rotating? Heron. 1989;34(1):1–59.
[23] Bazant ZP, Planas J. Fracture and Size Effect in Concrete and Other Quasibrittle Materials. CRC Press; 1998.
[24] Hordijk DA. Local Approach to Fatigue of Concrete: PhD thesis, Delft University of Technology; 1991.
[25] He W, Wu YF, Liew KM. A fracture energy based constitutive model for the analysis of reinforced concrete structures under cyclic loading. Comput Meth Appl Mech Eng.

2008;197(51-52):4745-62.
[26] Bizindavyi L, Neale KW, Erki MA. Experimental investigation of bonded fiber reinforced polymer-concrete joints under cyclic loading. J Compos Constr. 2003;7(2):127-34.
[27] Ferrier E, Bigaud D, Hamelin P, Bizindavyi L, Neale KW. Fatigue of CFRPs externally bonded to concrete. Mater Struct. 2005;38(275):39-46.
[28] Kim YJ, Heffernan PJ. Fatigue behavior of externally strengthened concrete beams with fiber-reinforced polymers: State of the art. J Compos Constr. 2008;12(3):246-56.
[29] Ko H, Sato Y. Bond stress-slip relationship between FRP sheet and concrete under cyclic load. J Compos Constr. 2007;11(4):419-26.
[30] Chen JF, Tao Y. Finite element modelling of FRP-to-concrete bond behaviour using concrete damage plasticity theory combined with a plastic degradation model. The 5th International Conference on FRP Composites in Civil Engineering (CICE 2010). Beijing, China2010. p. 45-50.
[31] Chen GM, Chen JF, Teng JG. On the finite element modelling of RC beams shear-strengthened with FRP. Construction and Building Materials (in press). 2011.
[32] Chen GM, Teng JG, Chen JF. Finite element modeling of intermediate crack debonding in FRP-plated beams. Journal of Composites for Construction, ASCE (in press). 2011.
[33] Niu H, Karbhari VM. FE investigation of material and preload parameters on FRP strengthening performance of RC beams, I: Model development. J Reinf Plast Compos. 2008;27(5):507-22.
[34] Niu HD, Karbhari VM, Wu ZS. Diagonal macro-crack induced debonding mechanisms in FRP rehabilitated concrete. Compos Pt B-Eng. 2006;37(7-8):627-41.
[35] Niu HD, Wu ZS. Numerical analysis of debonding mechanisms in FRP-strengthened RC beams. Comput-Aided Civil Infrastruct Eng. 2005;20(5):354-68.
[36] ABAQUS. ABAQUS 6.5 User's Manual. ABAQUS, Inc., Providence, RI.; 2004.
[37] Camanho PP, Davila CG. Mixed-Mode Decohesion Finite Elements for the Simulation of Delamination in Composite Materials. NASA/TM-2002–211737; 2002.
[38] Yuan H, Teng JG, Seracino R, Wu ZS, Yao J. Full-range behavior of FRP-to-concrete bonded joints. Eng Struct. 2004;26(5):553-65.

List of Figures

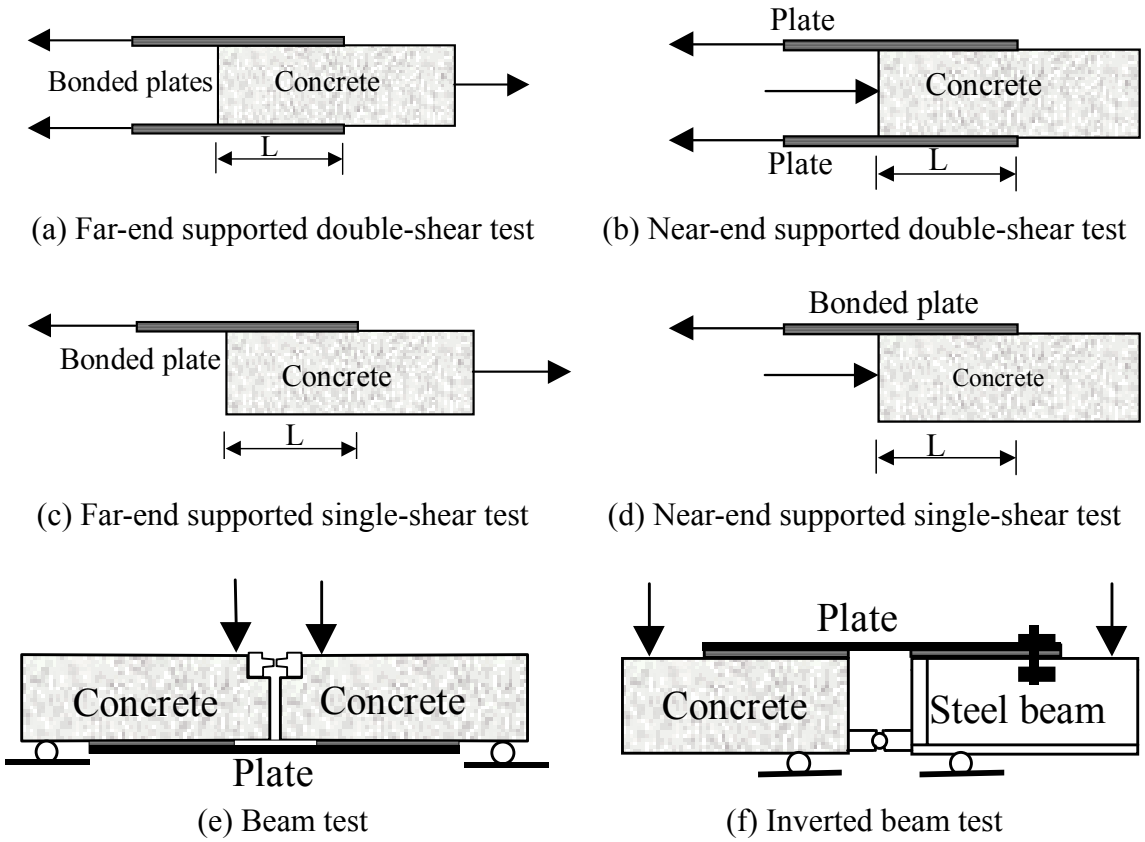

(a) Far-end supported double-shear test (b) Near-end supported double-shear test

(c) Far-end supported single-shear test (d) Near-end supported single-shear test

(e) Beam test (f) Inverted beam test

Fig. 1. Classification of bond tests [10,11]

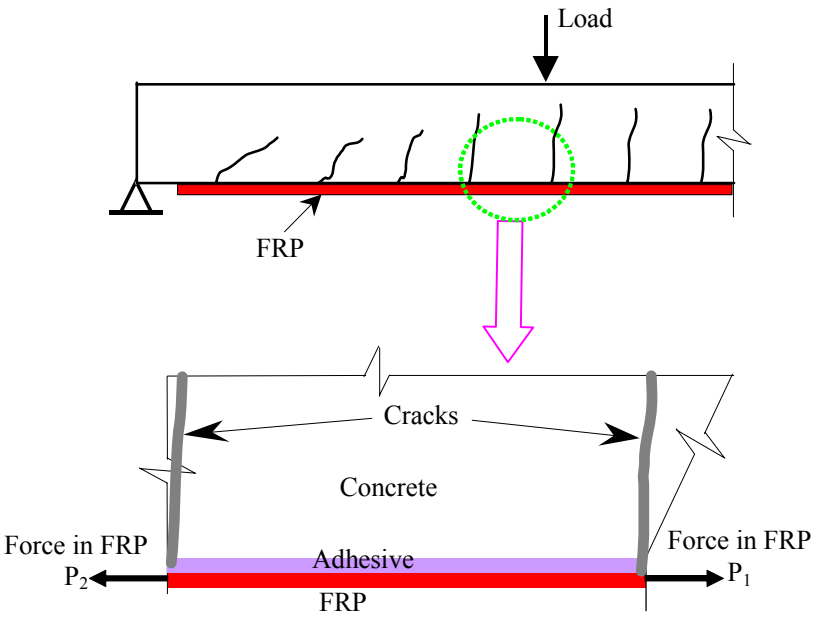

Fig. 2. Intermediate crack debonding in FRP-plated RC beams

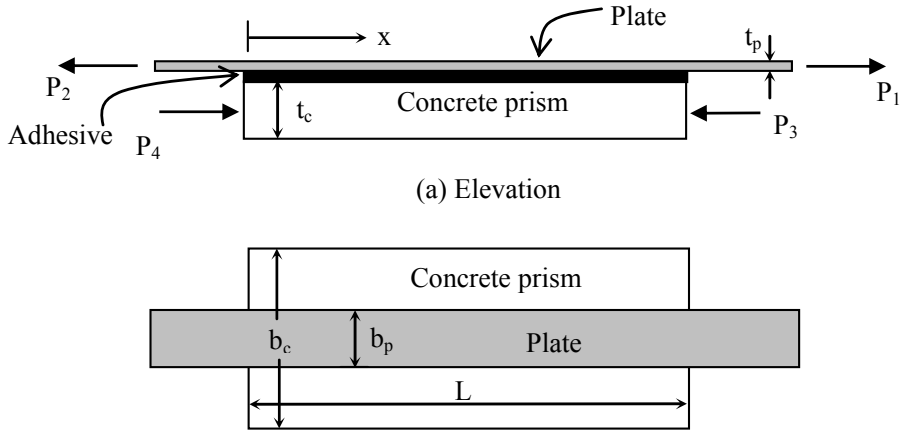

Fig. 3. FRP-to-concrete bonded joint model between two cracks

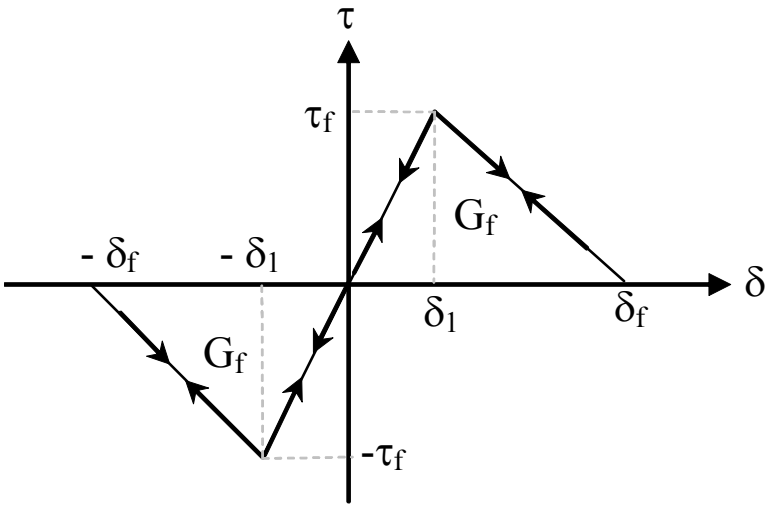

(a) Fully reversible bilinear bond-slip model

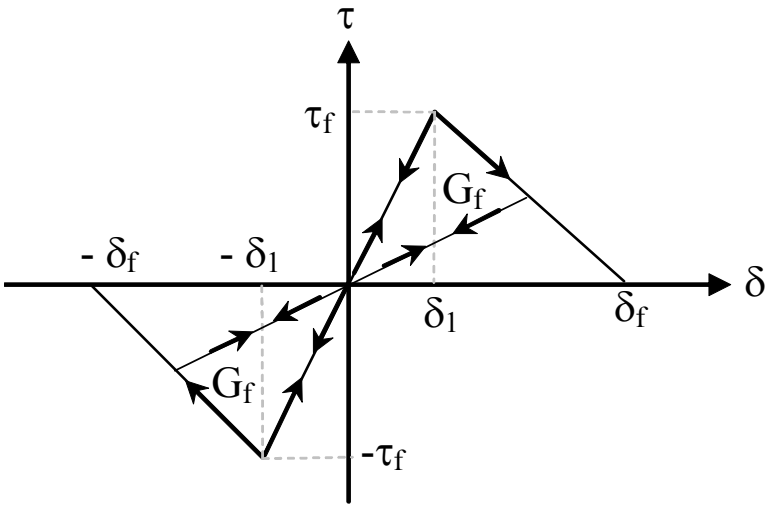

(b) Bilinear bond-slip model with linear damage

Fig. 4. FRP-concrete bond-slip models including unloading

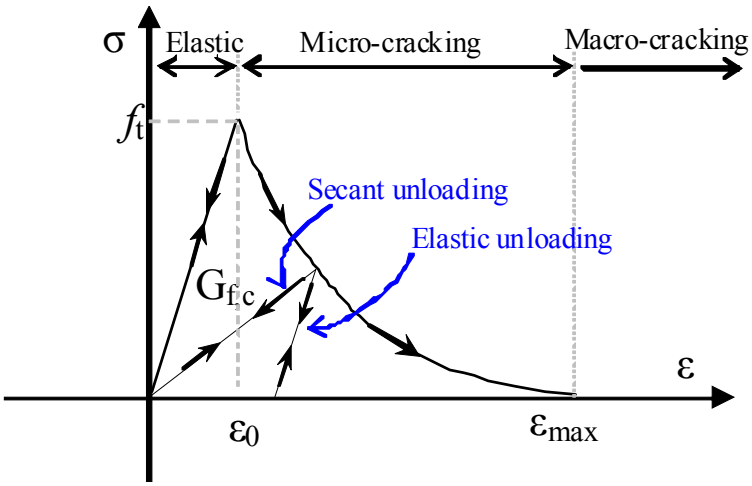

Fig. 5. Tensile stress-strain curve of concrete (adapted from Rots [21])

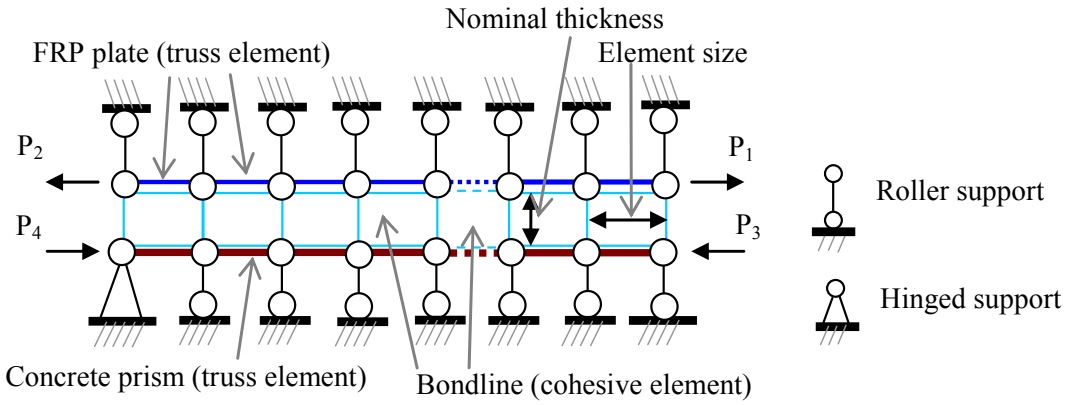

(a)

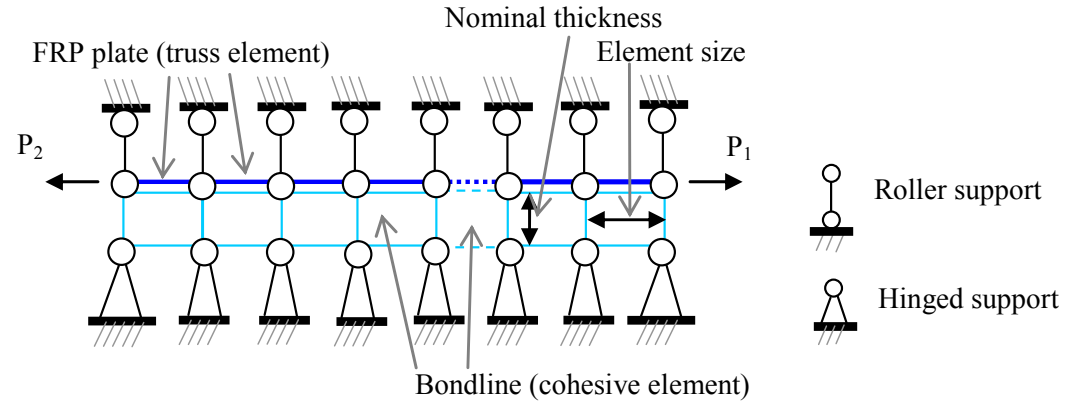

(b)

Fig. 6. The finite element model

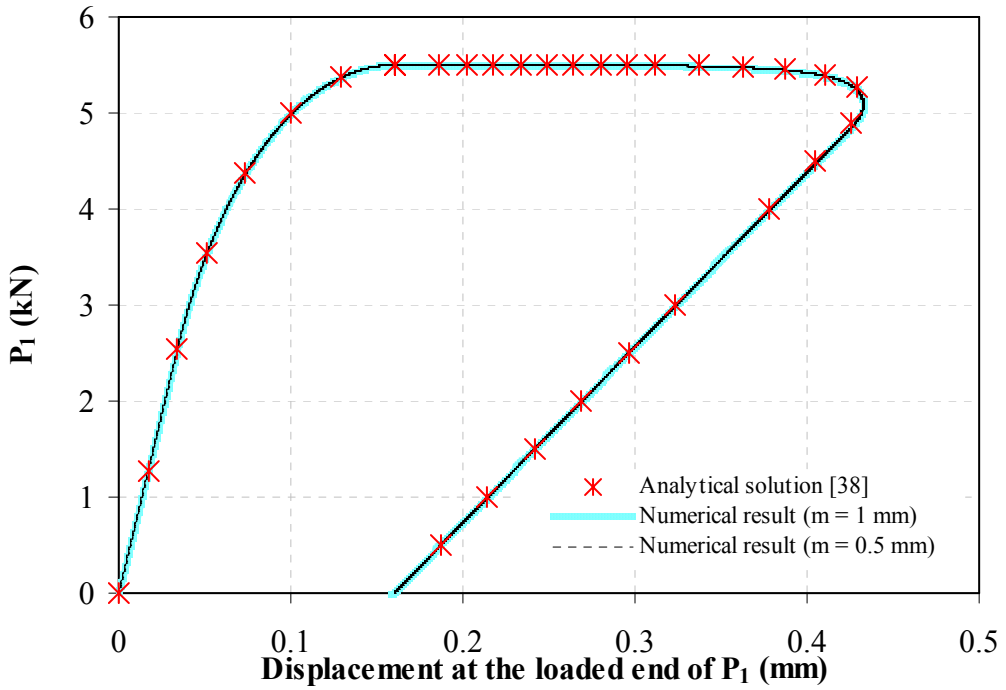

Fig. 7. Mesh convergence and comparison with analytical solution (L = 100 mm, β = 0)

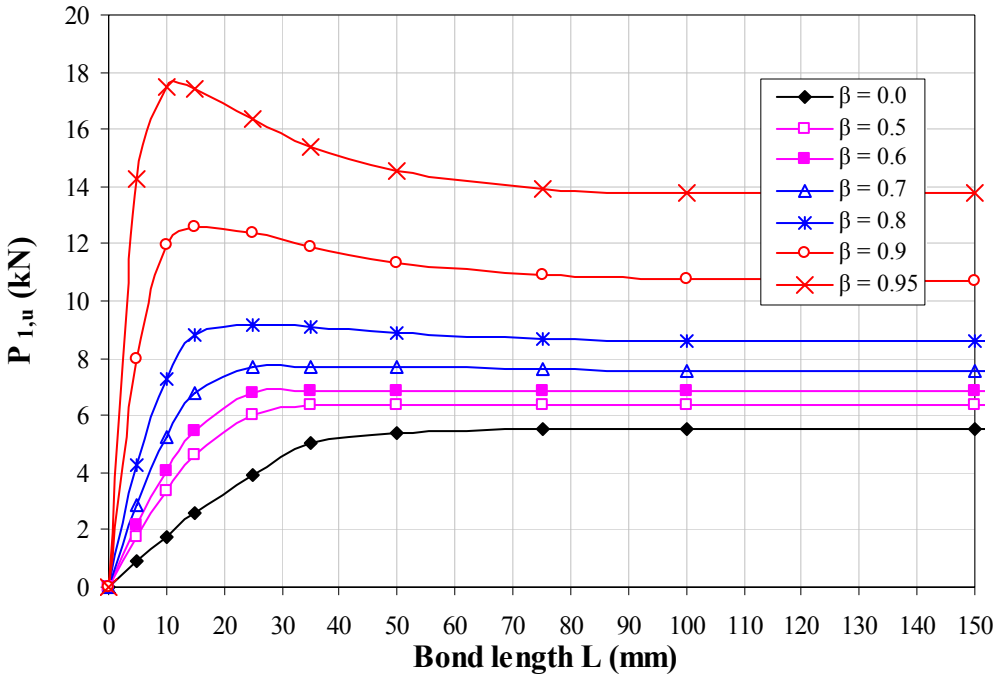

(a) Ultimate load $P_{1,u}$ versus bond length L

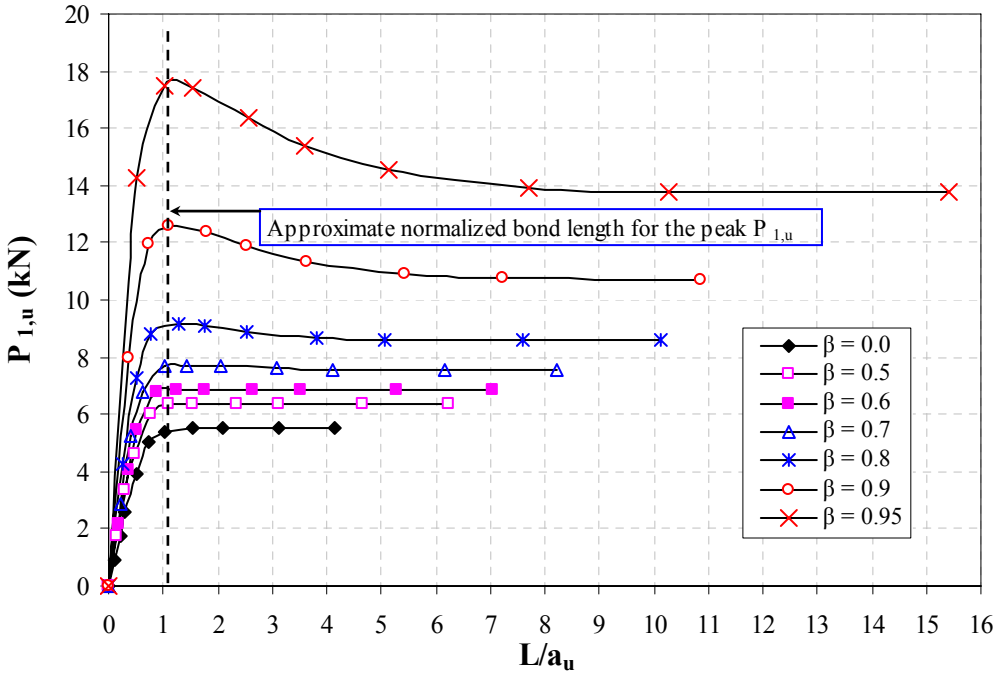

(b) Ultimate load $P_{1,u}$ versus normalised bond length L/a_u

Fig. 8. Effect of bond length L on the ultimate load $P_{1,u}$

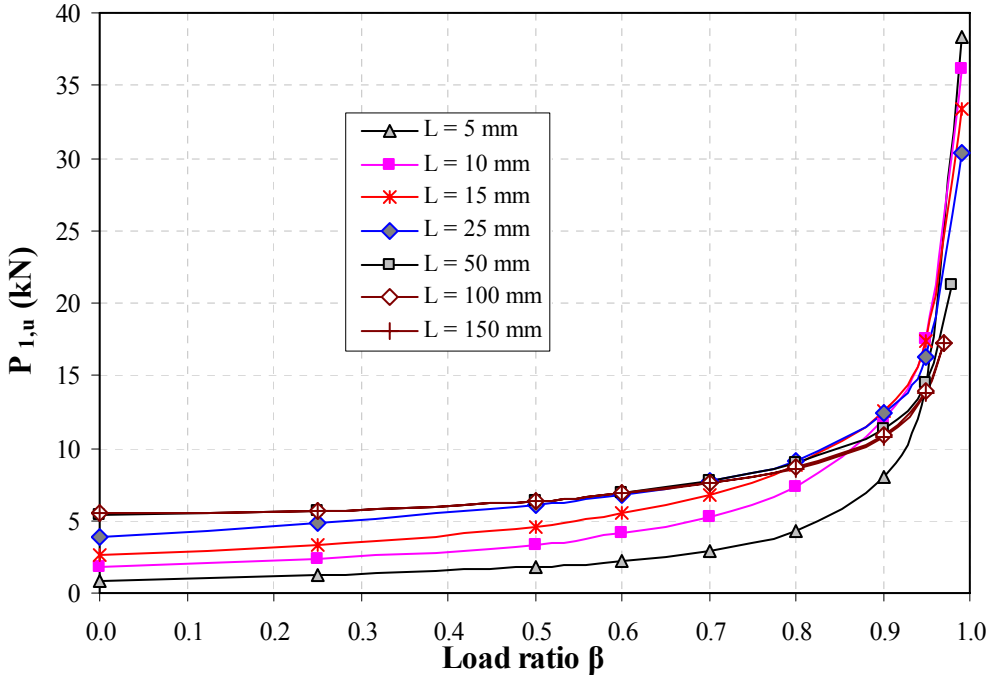

Fig. 9. Effect of load ratio β on the ultimate load $P_{1,u}$

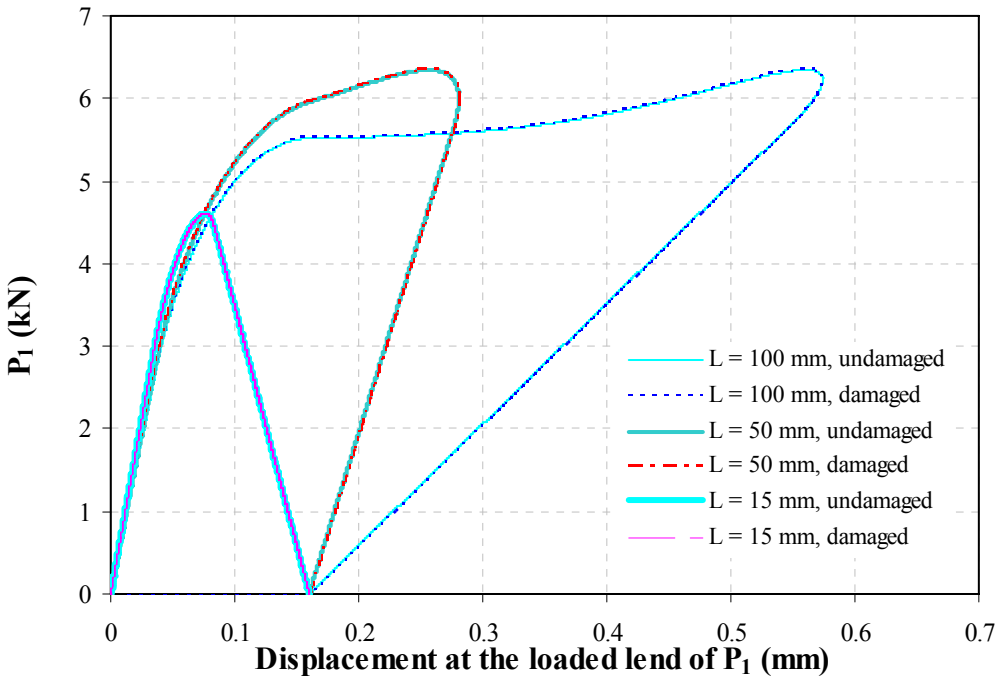

(a) $\beta = 0.5$

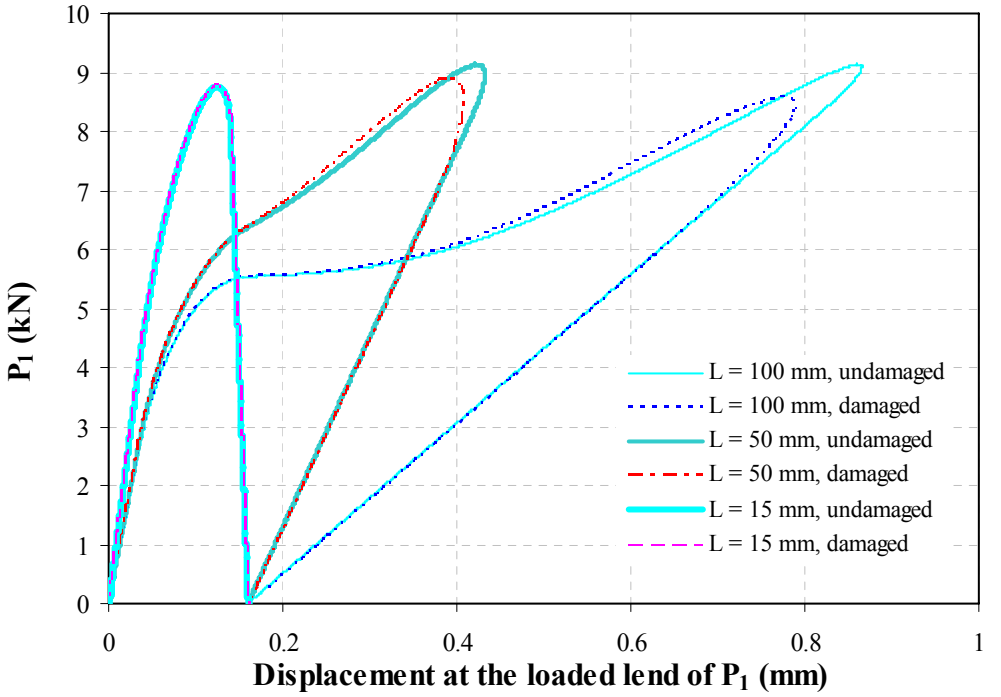

(b) $\beta = 0.8$

Fig. 10. Effect of damage on full-range load-displacement behaviour

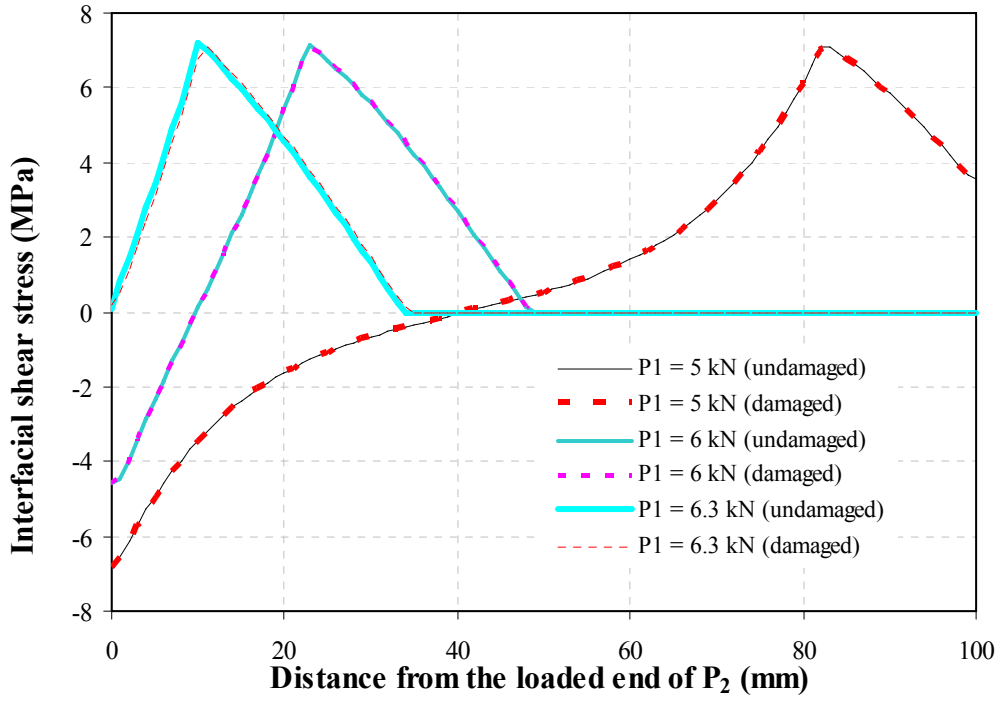

(a) $L = 100\,\text{mm}, \beta = 0.5$

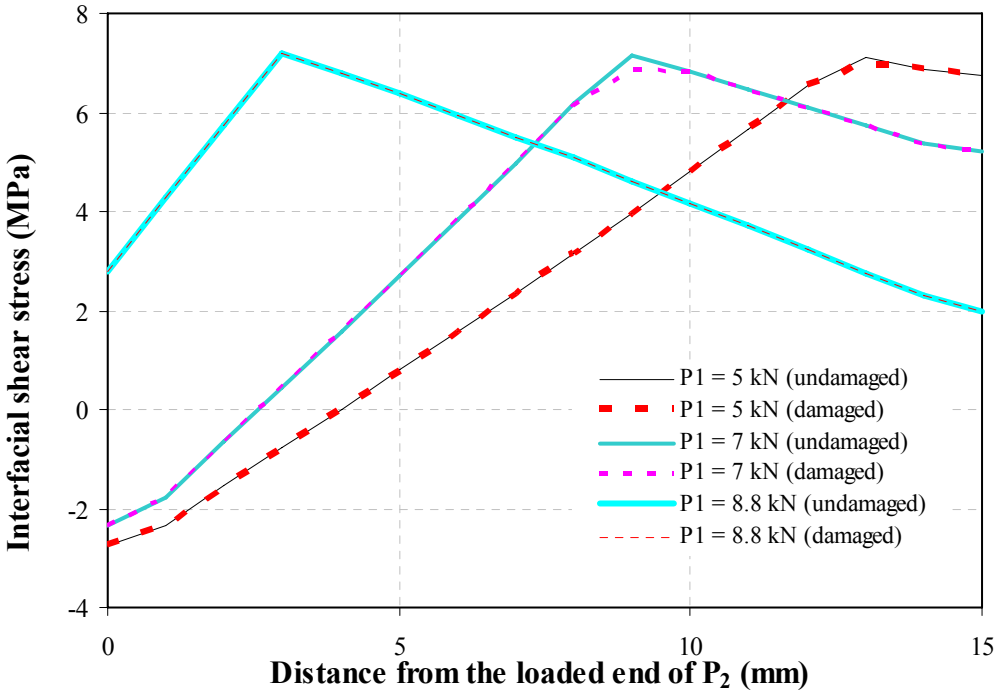

(b) $L = 15\,\text{mm}, \beta = 0.8$

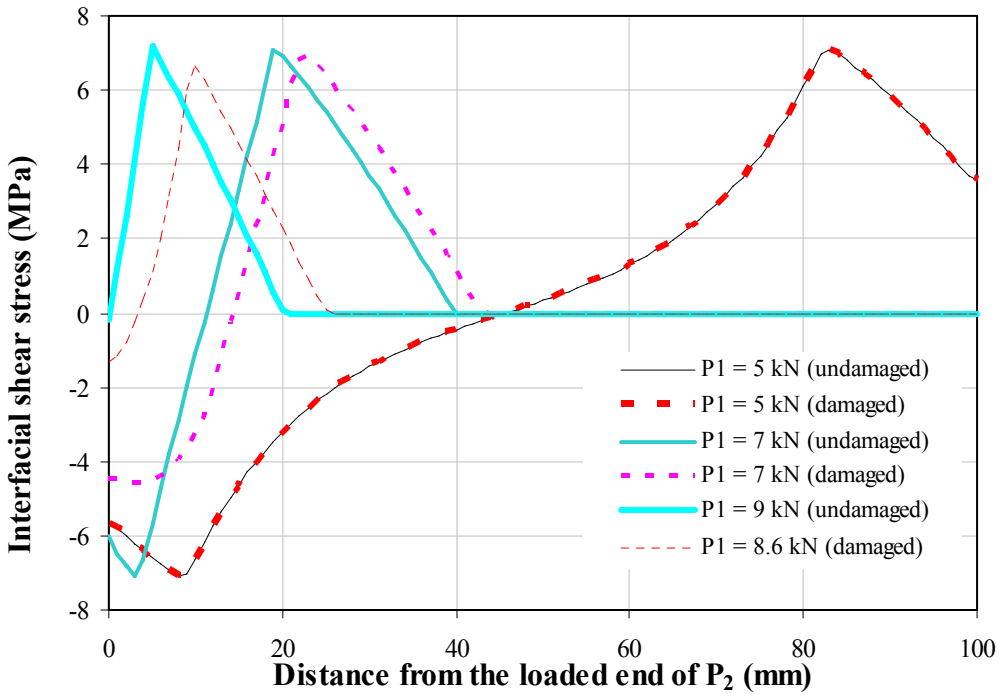

(c) $L = 100\,\text{mm}, \beta = 0.8$

Fig. 11. Effect of damage on interfacial shear stress distribution

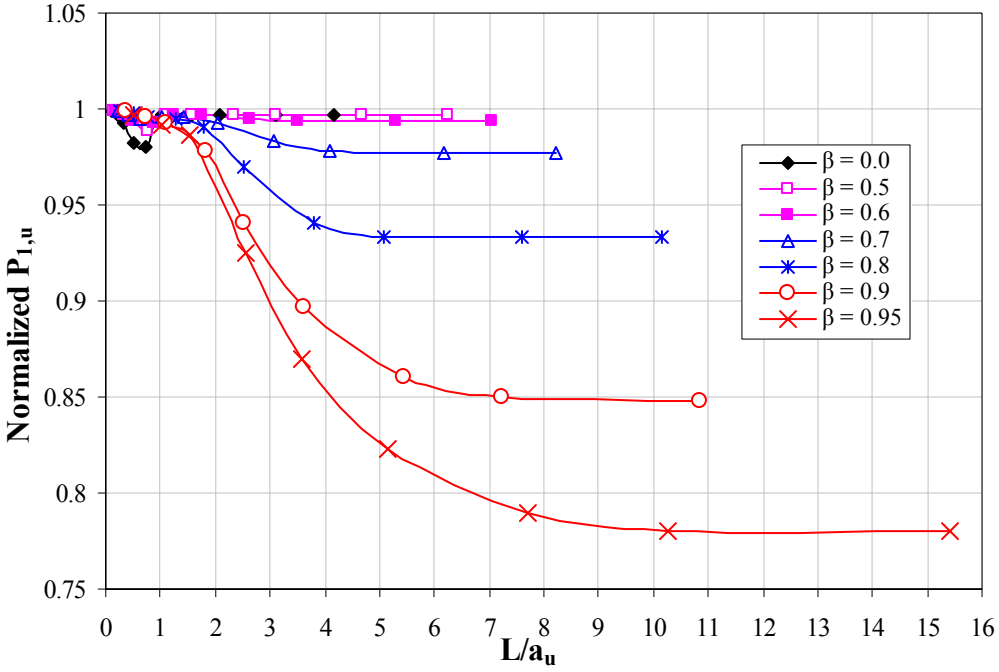

(a) Effect of normalized bond length L/a_u

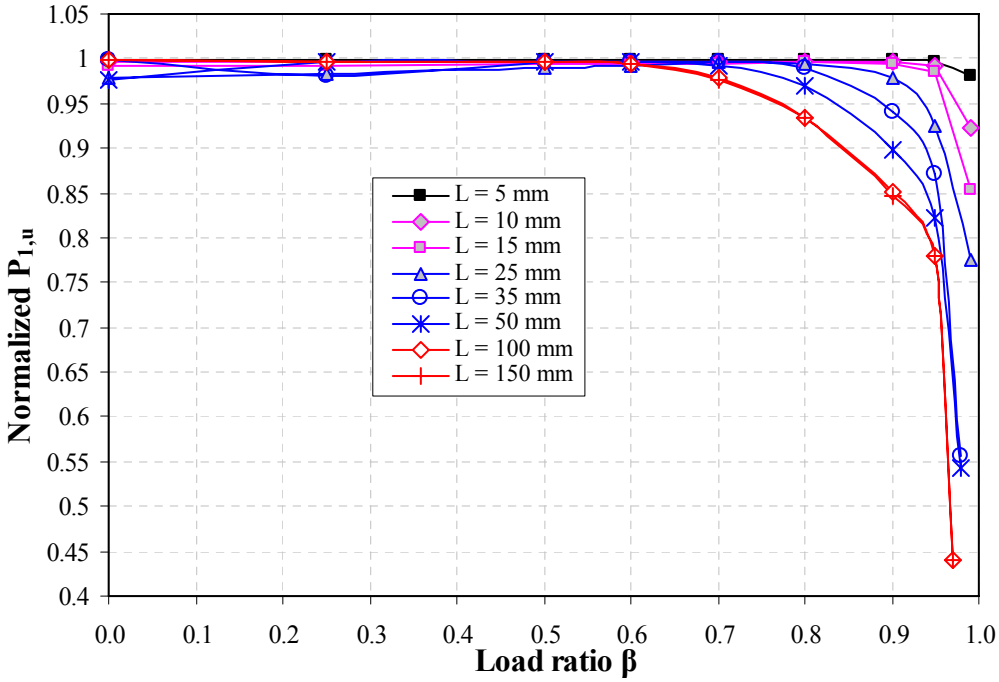

(b) Effect of load ratio β

Fig. 12. Numerical predictions versus Chen *et al.*'s [15] analytical solution